Optimal ignition placement in diffusion flames by nonlinear adjoint looping

By U. A. Qadri†, L. Magri, M. Ihme AND P. J. Schmid†

We derive and implement a gradient-based optimization framework to identify the best place to ignite a mixture of fuel and oxidizer. We have used the time-averaged increase in thermal energy as the cost function that indicates the success of ignition. We use direct numerical simulation (DNS) of the low Mach number Navier–Stokes equations with single-step finite-rate reaction chemistry to model spark ignition of an axisymmetric methane jet in air. We model the spark as a two-dimensional Gaussian function. We solve the adjoint of these equations to obtain the sensitivity of the cost function with respect to the position of the spark. We find that the optimal locations track the stoichiometric mixture fraction surface in the flow. At low Reynolds numbers, the optimization prefers locations downstream that allow upstream flame propagation.

1. Introduction

The combustion of fossil fuels is the main source of energy for transportation and power generation in the world today, and is expected to remain the case for the near future. The process of spark ignition of a turbulent mixture can generally be considered to have three stages (Mastorakos 2009). In the first stage, kernel generation, the spark leads to a localized flame kernel. In the second stage, flame expansion, the flame front propagates and spreads through the rest of the unburnt fluid. In the third stage, flame stabilization, the flame achieves a (statistically) steady and stable configuration.

Numerous studies have examined the factors that affect these stages of the ignition process (Mastorakos 2009). These studies, which are both experimental and numerical in nature, investigate the probability of successful ignition by carrying out a large number of individual spark trials and observing the final flame configuration. The results emphasize that the probability of ignition depends on many more factors than just the local mixture fraction profiles, which determine the flammability limits of the flow. The probability of all three stages being successful is not necessarily the same as the probability of kernel generation, which itself is not necessarily related to the flammability limits of the flow. The local strain rate, convection velocity, spark energy, spark size, and flow configuration all play a part in determining successful ignition.

Given the high sensitivity observed in experiments and simulations and the large number of degrees of freedom in the system, understanding the effect of the different factors on the process of ignition can be quite tedious, requiring a large number of parametric studies. One approach to overcome this challenge is to use ideas from optimal control theory. It involves formulating a constrained optimization problem for a suitable cost function of interest and using the adjoint operator to obtain gradient information cheaply in systems with a large number of degrees of freedom. This general approach has previously been used, for example, to optimize aircraft wing design (Jameson 1988), to understand and

† Imperial College London, UK

optimize mixing (Foures *et al.* 2013) and transition to turbulence (Pringle & Kerswell 2010), and to understand thermoacoustic instabilities in a simple model (Juniper 2011). Its application to the problem of ignition is significantly more complex.

The high sensitivity of ignition that has been observed in turbulent flows, as described above, is due not only to the stochastic nature of the turbulent flow. It has also been observed in laminar flames (Richardson & Mastorakos 2007). More recently, Capecelatro *et al.* (2016) used adjoints to calculate the sensitivity of ignition to several different parameters of the ignition process and identify the largest sources of uncertainty. In this project, we take this idea a step further and use the gradients provided by the adjoints as part of an optimization algorithm to find the 'best' place to ignite a gaseous mixture of fuel and oxidizer.

Experiments on ignition in turbulent flames (Mastorakos 2009) have found that the ignition probability in premixed flames is 100 % in large regions of the flow, whereas the ignition probability in non-premixed flames is high in small localized regions. As such, in this project, we focus on non-premixed flames because the competition between diffusion and reaction is more likely to produce localized optimals.

In Section 2, we describe the governing equations and formulate the nonlinear optimization problem in terms of the cost function of interest and the relevant constraints. In Section 3, we describe briefly the numerical implementation and flow configuration and present the results obtained during the summer program. Finally, in Section 4 we offer some conclusions and identify directions for future work.

2. Mathematical formulation

2.1. *Governing equations*

We treat the fuel and oxidizer as perfect gases and investigate the evolution of the flame in a domain Ω. The fluid in the domain has velocity $\mathbf{u} = (u_x, u_r, u_\theta)$, density ρ, pressure p, and temperature T. The concentration of the fuel is described using the mixture fraction Z, which has a value of $Z = 1$ for pure fuel and $Z = 0$ for pure oxidizer. We use the reacting low Mach number (LMN) equations as described by Nichols & Schmid (2008) to describe the motion of the fluid. In nondimensional form, these equations can be written as

$$\frac{\partial \rho}{\partial t} + \nabla \cdot (\rho \mathbf{u}) = 0,$$

$$\frac{\partial (\rho \mathbf{u})}{\partial t} = -\nabla p + \nabla \cdot (\frac{1}{S_1 \mathrm{Re}} \tau - \rho \mathbf{u} \mathbf{u}),$$

$$\rho(\frac{\partial Z}{\partial t} + \mathbf{u} \cdot \nabla Z) = \frac{1}{S_1 \mathrm{Re} \mathrm{Sc}} \nabla^2 Z, \qquad (2.1)$$

$$\rho(\frac{\partial T}{\partial t} + \mathbf{u} \cdot \nabla T) = \frac{1}{S_1 \mathrm{Re} \mathrm{Pr}} \nabla^2 T + Da \rho^3 \omega,$$

$$\rho \left[(S_1 - 1)Z + 1\right] \left[(S_2 - 1)T + 1\right] = 1,$$

where $\tau = \left[\nabla \mathbf{u} + (\nabla \mathbf{u})^T\right] - \frac{2}{3}(\nabla \cdot \mathbf{u})I$ is the non-isotropic component of the rate-of-strain tensor. We have neglected body forces and assumed Fourier's law of conduction. We assume that the effects of buoyancy are negligible and that the viscosity, thermal diffusivity, mass diffusivity and specific heat capacity are uniform throughout the flow. The Prandtl number, Pr, and Schmidt number, Sc, then describe the ratio of the diffusivity of temperature and mass, respectively, to the diffusivity of momentum.

The flow variables have been nondimensionalized by using a suitable reference length and velocity scale based on the fuel and the oxidizer density. These scales depend on the flow configuration being considered and are defined in Section 3. The Reynolds number, Re, however, is defined in terms of the fuel density. This definition introduces a $1/S_1$ factor in front of the viscous terms in Eq. (2.1). The nondimensional temperature is defined as $T = (T^* - T_0)/(T_f - T_0)$, where T^* (K) is the dimensional temperature, T_f is the dimensional adiabatic flame temperature, and T_0 is the dimensional ambient oxidizer temperature. The ratio of the oxidizer density to fuel density defines the density ratio parameter, S_1. The source term, $\text{Da}\rho^3\omega$, is equivalent to the nondimensional rate of enthalpy release per unit volume. For the rate of reaction, ω, we use a one-step chemistry mechanism described by the Arrhenius law

$$\omega = \left\{ \left(Z - \frac{T}{s+1} \right) \left(1 - Z - \frac{sT}{s+1} \right) - \kappa T^2 \right\} \exp\left[\frac{-\beta(1-T)}{1 - \alpha(1-T)} \right]. \qquad (2.2)$$

The chemistry of the reaction is described by the mass stoichiometric ratio, s, the equilibrium constant, κ, the heat release parameter, $\alpha \equiv (T_f - T_0)/T_f$, and the Zeldovich number $\beta \equiv \alpha T_a/T_f$, where T_a (K) is the dimensional activation temperature of the reaction, and T_f (K) is the dimensional adiabatic flame temperature. The ratio of the adiabatic flame temperature to the oxidizer temperature at the inlet defines the temperature ratio parameter, $S_2 \equiv T_f/T_0$.

2.2. *Variational framework*

The governing equations describe the evolution of the state vector, $q(x_i, t) \equiv [m_i, Z, T, \rho]^T$, where $m_i = \rho u_i$ is the momentum, starting from an initial condition $q(x_i, t = 0) = q_0(x_i)$. We seek to find the initial condition q_0 that maximizes a cost function $\mathcal{J}$. This cost function should be a good measure of successful ignition. In this study, we use the time-averaged temperature as a measure of successful ignition. This has been shown to be suitable for optimization over short times following ignition (Capecelatro *et al.* 2016). The cost function is given by

$$\mathcal{J} = \frac{1}{2V} \int_{t=0}^{t=\tau} \int_{\Omega} T^2 dV \, dt, \qquad (2.3)$$

where V is the volume of the domain Ω. This cost function is constrained by the governing equations, Eq. (2.1), and by the initial condition q_0. The optimization problem can then be posed as the Lagrangian

$\mathcal{L} =$

$$\mathcal{J}(T) - \left\langle m_i^+, \, \frac{\partial m_i}{\partial t} + \frac{\partial p}{\partial x_i} + \frac{\partial}{\partial x_j}\left(\frac{m_i m_j}{\rho} \right) - \frac{S_1^{-1}}{\text{Re}} \left(\frac{\partial^2}{\partial x_j^2}\left(\frac{m_i}{\rho} \right) + \frac{1}{3}\frac{\partial}{\partial x_j \partial x_i}\left(\frac{m_i}{\rho} \right) \right) \right\rangle$$

$$- \left\langle Z^+, \, \rho\frac{\partial Z}{\partial t} + m_i\frac{\partial Z}{\partial x_i} - \frac{S_1^{-1}}{\text{ReSc}}\frac{\partial^2 Z}{\partial x_i^2} \right\rangle - \left\langle T^+, \, \rho\frac{\partial T}{\partial t} + m_i\frac{\partial T}{\partial x_i} - \frac{S_1^{-1}}{\text{RePr}}\frac{\partial^2 T}{\partial x_i^2} - \text{Da}\rho^3\dot{\omega} \right\rangle$$

$$- \left\langle p^+, \, \frac{\partial \rho}{\partial t} + \frac{\partial m_i}{\partial x_i} \right\rangle - \left\langle \rho^+, \, \rho\left[(S_1 - 1)Z + 1\right]\left[(S_2 - 1)T + 1\right] - 1 \right\rangle - \left[q_0^+, \, q(\mathbf{x}, 0) - q_0 \right],$$

$$(2.4)$$

where the inner products are defined as

$$\langle a, b \rangle = \int_{t=0}^{t=\tau} \frac{1}{V} \int_\Omega a^T b \, dV \, dt$$

$$[a, b] = \frac{1}{V} \int_\Omega a^T b \, dV. \tag{2.5}$$

The adjoint variables $q^+(x_i, t) \equiv [m_i^+, Z^+, T^+, \rho^+]^T$ act as Lagrange multipliers and enforce the constraints described by the governing equations. When the cost function is maximized, $\delta \mathcal{J} = 0$ by definition. In the constrained problem, this is achieved by setting first variations with respect to all variables to zero. This produces a set of equations that describes the evolution of the adjoint fields. Following Chandler *et al.* (2012) and Qadri *et al.* (2015), to ensure numerical stability of the adjoint equations, the expression in Eq. (2.4) is first rearranged to remove the unsteady term in the continuity equation,

$$\mathcal{L} =$$

$$\mathcal{J} - \left\langle m_i^+, \frac{\partial m_i}{\partial t} + \frac{\partial p}{\partial x_i} + \frac{\partial}{\partial x_j}\left(\frac{m_i m_j}{\rho}\right) - \frac{S_1^{-1}}{\mathrm{Re}}\left(\frac{\partial^2}{\partial x_j^2}\left(\frac{m_i}{\rho}\right) + \frac{1}{3}\frac{\partial^2}{\partial x_j \partial x_i}\left(\frac{m_i}{\rho}\right)\right)\right\rangle$$

$$- \left\langle Z^+, \frac{\partial Z}{\partial t} + \frac{m_i}{\rho}\frac{\partial Z}{\partial x_i} - \frac{S_1^{-1}}{\mathrm{ReSc}\rho}\frac{\partial^2 Z}{\partial x_i^2}\right\rangle - \left\langle T^+, \frac{\partial T}{\partial t} + \frac{m_i}{\rho}\frac{\partial T}{\partial x_i} - \frac{S_1^{-1}}{\mathrm{RePr}\rho}\frac{\partial^2 T}{\partial x_i^2} - \mathrm{Da}\rho^2\dot{\omega}\right\rangle$$

$$- \left\langle p^+, \frac{\partial}{\partial x_i}\left(\frac{m_i}{\rho}\right) - \frac{K_2}{S_1\mathrm{ReSc}}\frac{\partial^2 Z}{\partial x_i^2} - K_1\left(\frac{1}{S_1\mathrm{RePr}}\frac{\partial^2 T}{\partial x_i^2} + \mathrm{Da}\rho^3\dot{\omega}\right)\right\rangle$$

$$- \left\langle \rho^+, \rho\left[(S_1-1)Z+1\right]\left[(S_2-1)T+1\right] - 1 \right\rangle - \left[q_0^+, q(\mathbf{x}, 0) - q_0\right], \tag{2.6}$$

where $K_1 = (S_2-1)[(S_1-1)Z+1]$ and $K_2 = (S_1-1)[(S_2-1)T+1]$. Taking first variations with respect to the flow variables, we express the linearization of the reaction term and density as

$$\delta\dot{\omega} = K_Z\delta Z + K_T\delta T \tag{2.7}$$

$$\delta\rho = -\rho^2(K_1\delta T + K_2\delta Z). \tag{2.8}$$

This yields the adjoint equations

$$\frac{\delta\mathcal{L}}{\delta m_i} = 0 \Longrightarrow -\frac{\partial m_i^+}{\partial t} - \frac{1}{\rho}\frac{\partial p^+}{\partial x_i} - \frac{m_j}{\rho}\left(\frac{\partial m_i^+}{\partial x_j} + \frac{\partial m_j^+}{\partial x_i}\right)$$

$$- \frac{1}{S_1\mathrm{Re}\rho}\left(\frac{\partial^2 m_i^+}{\partial x_j^2} + \frac{1}{3}\frac{\partial^2 m_j^+}{\partial x_j \partial x_i}\right) + \frac{T^+}{\rho}\frac{\partial T}{\partial x_i} + \frac{Z^+}{\rho}\frac{\partial Z}{\partial x_i} := 0 \tag{2.9}$$

$$\frac{\delta\mathcal{L}}{\delta Z} = 0 \Longrightarrow -\frac{\partial Z^+}{\partial t} - m_i\frac{\partial}{\partial x_i}\left(\frac{Z^+}{\rho}\right) - \frac{Z^+}{\rho}\frac{\partial m_i}{\partial x_i} - \frac{1}{S_1\mathrm{ReSc}}\frac{\partial^2}{\partial x_i^2}\left(\frac{Z^+}{\rho} + K_2 p^+\right)$$

$$- \left[\frac{(S_2-1)(S_1-1)}{S_1\mathrm{RePr}}\frac{\partial^2 T}{\partial x_i^2} + (S_2-1)(S_1-1)\mathrm{Da}\rho^3\dot{\omega}\right]p^+$$

$$- \mathrm{Da}\rho^3\left(\frac{T^+}{\rho} + K_1 p^+\right)K_Z + K_2\rho\rho^+ = 0 \tag{2.10}$$

$$\frac{\delta \mathcal{L}}{\delta T} = 0 \Longrightarrow -\frac{\partial T^+}{\partial t} - m_i \frac{\partial}{\partial x_i} \left(\frac{T^+}{\rho} \right) - \frac{T^+}{\rho} \frac{\partial m_i}{\partial x_i} - \frac{1}{S_1 \text{RePr}} \frac{\partial^2}{\partial x_i^2} \left(\frac{T^+}{\rho} + K_1 p^+ \right)$$

$$- \left[\frac{(S_2-1)(S_1-1)}{S_1 \text{ReSc}} \frac{\partial^2 Z}{\partial x_i^2} \right] p^+$$

$$- \text{Da}\rho^3 \left(\frac{T^+}{\rho} + K_1 p^+ \right) K_T + K_1 \rho \rho^+ - T = 0 \qquad (2.11)$$

$$\frac{\delta \mathcal{L}}{\delta \rho} = 0 \Longrightarrow \frac{m_i m_j}{\rho^2} \frac{\partial m_i^+}{\partial x_j} + \frac{m_i}{S_1 \text{Re}\rho^2} \left(\frac{\partial^2 m_i^+}{\partial x_j^2} + \frac{1}{3} \frac{\partial^2 m_j^+}{\partial x_j \partial x_i} \right) + \frac{m_i}{\rho^2} \frac{\partial p^+}{\partial x_i}$$

$$- \frac{Z^+}{\rho^2} \left(m_i \frac{\partial Z}{\partial x_i} - \frac{1}{S_1 \text{ReSc}} \frac{\partial^2 Z}{\partial x_i^2} \right) - \frac{T^+}{\rho^2} \left(m_i \frac{\partial T}{\partial x_i} - \frac{1}{S_1 RePr} \frac{\partial^2 T}{\partial x_i^2} + 2\text{Da}\rho^3 \dot{\omega} \right)$$

$$- 3\text{Da}\rho^2 K_1 \dot{\omega} p^+ + \frac{\rho^+}{\rho} = 0. \qquad (2.12)$$

The adjoint equations have to be solved backward in time from $t = \tau$ to $t = 0$. Integrating the time derivatives produces additional terms that are used to initialize the adjoint based on the form of the cost functional and the initial conditions. For our choice of cost function, the initial conditions for the adjoint are all zero, $m_i^+(\tau) = Z^+(\tau) = T^+(\tau) = 0$, but we have an additional term forcing the adjoint temperature equation. Alternatively, optimizing based on the final temperature would give us

$$\mathcal{J} = \frac{1}{V} \int_\Omega \frac{1}{2} T(\tau)^2 dV \Longrightarrow m_i^+(\tau) = Z^+(\tau) = 0, \ T^+(\tau) = T(\tau). \qquad (2.13)$$

The first variation with respect to the initial conditions provides the gradient that we are interested in. This is given by the adjoint field at $t = 0$,

$$\frac{\delta \mathcal{L}}{\delta q_0} = 0 \Longrightarrow \frac{\delta L}{\delta q_0} = q^+(t = 0). \qquad (2.14)$$

The gradient describes how the initial condition should be changed to maximize the cost function. In this study, the initial condition is a spark, modeled as a Gaussian with amplitude A and width in each direction Δ_i in the temperature field at location s_i,

$$T_0(x_i) = T(x_i, \ t = 0) = A \exp \left[-\frac{(x_i - s_i)^2}{\Delta_i^2} \right], \qquad (2.15)$$

where the indices indicate summation over the number of spatial dimensions. Using the chain rule, the gradient for the spark position is given by

$$\frac{\delta \mathcal{L}}{\delta s_i} = \frac{\delta \mathcal{L}}{\delta T_0} \frac{\partial T_0}{\partial s_i} = T^+(t = 0) \frac{\partial T_0}{\partial s_i}. \qquad (2.16)$$

This gradient can then be used with a suitable optimization algorithm to arrive at an optimal spark position $s_i^{(opt)}$.

3. Flow configuration and results

We now apply the framework described in the previous section to study an axisymmetric jet of fuel containing 50% H_2 and 50% N_2 exiting into a cylindrical domain filled with air. For this fuel-oxidizer combination, $S_1 = 1.92$, $S_2 = 6.88$, and $s = 8$, and we set $\beta = 3$, $\kappa = 0.01$, and $\text{Pr} = \text{Sc} = 0.7$. We use the jet diameter, D, and jet axial velocity as reference scales and consider flow at $\text{Re} = 200$ with $\text{Da} = 100000$.
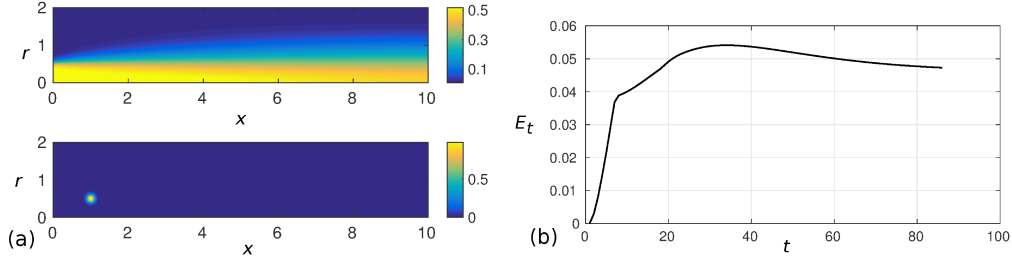
FIGURE 1. (a) The non-reacting base flow, showing contours of (top) axial momentum and (bottom) temperature used as the initial condition, (b) the evolution of the thermal energy $E_t = \frac{1}{V} \int_\Omega T^2 \, dV$ with time during the ignition process.

3.1. *Numerical solution*

We use an axisymmetric DNS code (Qadri *et al.* 2015) to solve the governing equations. A fourth-order Runge-Kutta scheme is used to march the discretized equations forward in time. The equations are discretized in space using a sixth-order compact finite difference scheme. We use a grid with 255×513 points for a cylindrical domain measuring 8.0×10.0 jet diameters in the radial and axial directions, respectively. We find this to produce results that are well converged and well resolved based on previous simulations (Qadri *et al.* 2015).

Along the lateral boundary, $r/D = 4.0$, we use a viscous traction free boundary condition for the momentum and set $T = 0$ and $Z = 0$. At the outlet boundary, $x/D = 10.0$, we use a convective boundary condition for the momentum, temperature and mixture fraction. These boundary conditions model flow into a semi-infinite domain in the downstream and radial directions. The pressure-projection scheme used in the code uses a discrete cosine transform to set boundary conditions for the pressure at the inlet and outlet boundaries. We use a half-wave cosine transform, which sets $dp/dx = 0$ at the inlet and outlet boundaries. Along the lateral boundary, we set $p = 0$. At the inlet boundary, we set the axial velocity and mixture fraction to have a top-hat profile. The temperature profile at the inlet is set to be uniform.

3.2. *Flow characterization*

Before we proceed with optimizing the ignition placement, we find it useful to simulate the ignition process. We obtain a non-reacting base flow setting $Da = 0$, shown in Figure 1(a). We 'ignite' the flow by imposing a 2-D Gaussian on the temperature field at a nominal location $(s_x, s_r) = (2.0, 0.5)$ and observe how the flame develops. In this axisymmetric flow configuration, our ignition model corresponds to a ring rather than a point source. In Figure 1(b), we plot the l_2 norm of the temperature field at each point in time. The cost function, Eq. (2.3), corresponds to the area underneath this curve. We notice that the thermal energy rises rapidly and then levels off and achieves a steady state. Comparing this curve with Figure 2, we notice that the initial rapid rise corresponds to the flame growing through the flow (Figure 2(ab)). Once the flame has grown through the entire numerical domain, the thermal energy begins to level off (Figure 2(c)) and the flame adjusts and stabilizes to reach a steady state (Figure 2(d)).

3.3. *Gradient information*

In their study on ignition in a mixing layer, Capecelatro *et al.* (2016) found that solving the governing equations over a short time frame after spark placement produced robust
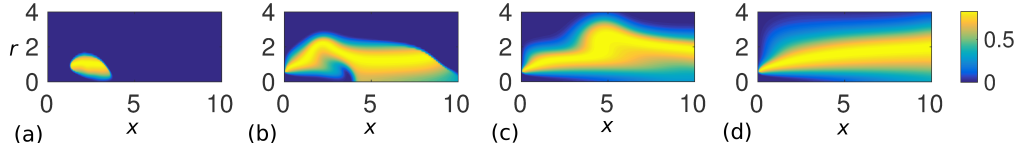
FIGURE 2. The evolution of the temperature field with time during the ignition process, from left to right, (a) $t = 1$, (b) $t = 5$, (c) $t = 20$, (d) $t = 60$.
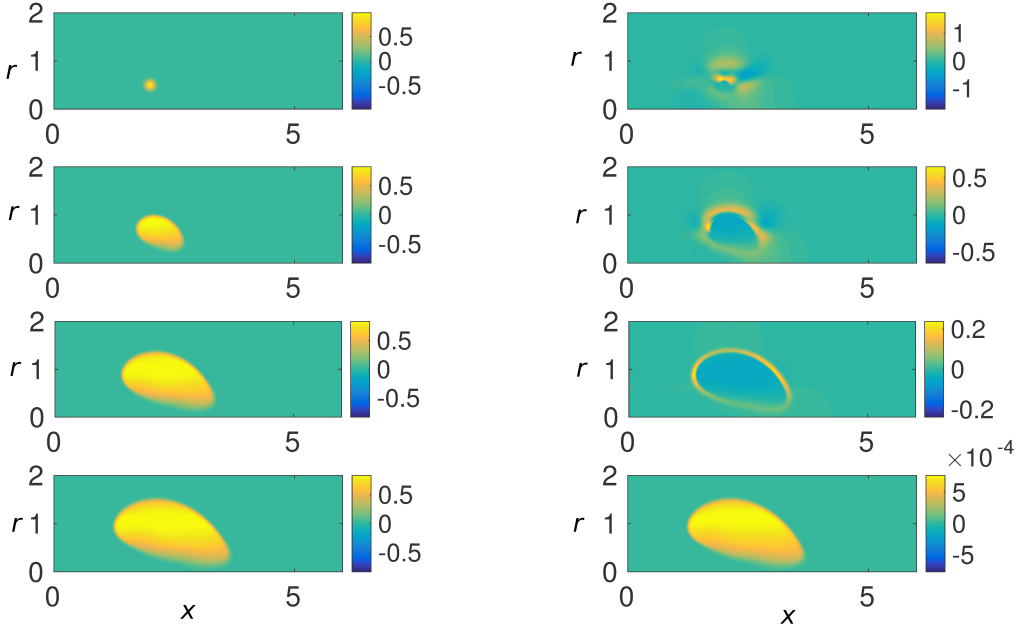

FIGURE 3. The evolution of the (left) temperature and (right) adjoint temperature fields with time during the ignition process, from top to bottom, $t = 0$, $t = 0.4$, $t = 0.8$, and $t = 1.0$.

sensitivity gradients. We solve the governing equations forward in time and the adjoint equations backward in time for $0 < t < \tau$. In Figure 3, we plot the evolution of the temperature and adjoint temperature fields for $\tau = 1.0$. At each point in time, the adjoint field identifies the most sensitive regions in the flow. These are the regions where a small change produces the largest effect on the cost function. We notice that, at intermediate times at which the flame is growing, the adjoint fields have large magnitudes around the flame front. This makes physical sense because the reaction rates and thermal gradients are high here. The adjoint temperature field at $t = 0$ provides information on the sensitivity of the initial condition. We notice that this field is not as localized as the initial condition itself. It identifies regions downstream and radially outward that are influential compared with the original spark position. A rough interpretation of this field is to deduce that moving the spark to a lighter region in the figure will increase the cost function, whereas moving the spark to a darker region in the figure will decrease the cost function. A more quantitative interpretation can be obtained by calculating the gradient in Eq. (2.16). This gradient vector has two components, an axial component and a radial component. For this flow, we find that the gradient in the radial direction is an order of magnitude larger than the gradient in the axial direction.
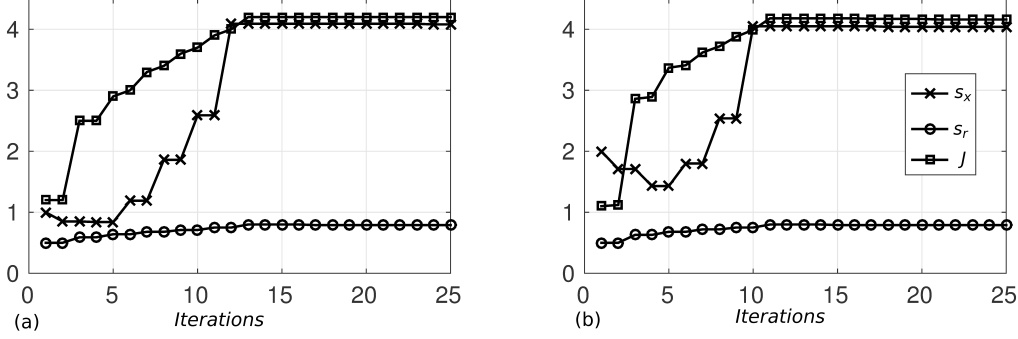
FIGURE 4. The convergence of the cost function $\mathcal{J}$ (squares), axial position (crosses) and radial position (circles) of the spark during an optimization loop starting from (a) $(s_x, \ s_r) = (1.0, 0.5)$ (left) and (b) $(s_x, \ s_r) = (2.0, 0.5)$ (right).

3.4. *Optimization of ignition location*

We use this gradient as part of an iterative optimization algorithm to converge toward an optimal location. We found that a standard steepest ascent or conjugate gradient algorithm did not converge efficiently toward an optimal. This is due to the inherent bias in the gradient vector—the radial component is much larger than the axial component. This is because the mixture fraction and flow properties vary weakly in the axial direction but vary strongly in the radial direction. To overcome this limitation, we used a hybrid algorithm in which we applied the steepest ascent approach (with line-search) alternately in the axial and radial directions. In one step, we updated the axial position of the spark, and in the next step, we updated the radial position of the spark. At each step, the new initial condition is normalized to maintain the same spark energy, $E_s = \frac{1}{V} \int_\Omega T_0^2 dV$.

Figure 4 shows the results of the optimization procedure for a short time-period $\tau = 0.1$, starting from two different initial conditions. In both cases, the algorithm converges to the same position $(4.05, 0.79)$, which we interpret as a local optimal. To understand the physical significance of this result, we follow an alternative optimization strategy where we fix the axial position and find the optimal radial position at each axial location. The results of this optimization procedure are shown in Figure 5. We notice that the optimal ignition locations are close to the stoichiometric mixture fraction surface. The optimization algorithm prefers ignition on the lean side of the stoichiometric surface. One explanation for this is that the scalar dissipation rate is maximal at $Z = 0.5$, which is on the lean side of the stoichiometric surface. This also explains why, in Figure 4, the algorithm selects a location upstream before it moves downstream. The initial conditions at $(2.0, 0.5)$ and $(1.0, 0.5)$ are well into the rich side of the mixture fraction. The first step corresponds to a step in the streamwise direction. The algorithm chooses to go upstream because this is where it is more likely to find the most reactive mixture or the stoichiometric mixture at $r = 0.5$. Going downstream, the stoichiometric mixture would be at a larger value of r. It is also interesting that the cost function increases more gently farther downstream. Increasing the value of τ over which the optimization is carried out also tends to favor locations farther downstream. We have checked that the results are not spurious, and the flame ignites successfully even when the spark is placed at axial locations $x/D > 7.0$. In this case, this is because this flow configuration and low Reynolds number allow upstream flame propagation. There is, therefore, a greater increase in thermal energy if the flame grows upstream as well as downstream. This result
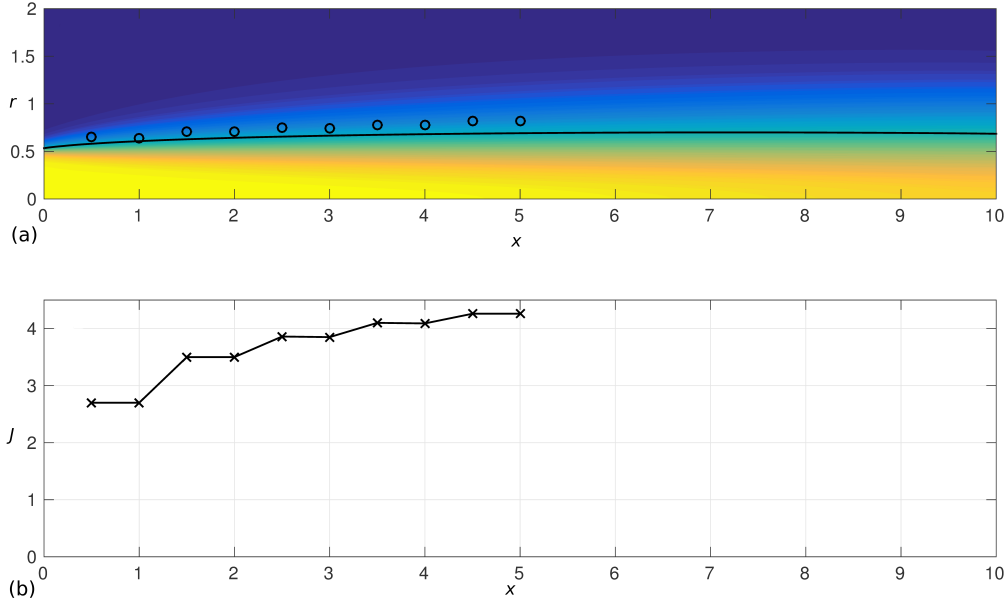
FIGURE 5. (a) The optimal spark position (circle) at various axial locations downstream of the inlet plane with contours of axial momentum of the non-reacting flow. The black line represents the stoichiometric surface $Z_{st} = 0.306$ for this fuel-oxidizer combination. (b) The cost function at the spark positions shown in (a).

is not general, however, and we expect that at higher Reynolds numbers, and in flows with recirculation, such as bluff-body or swirl-stabilized flames, we would find strong localization in the axial direction as well. This can also be checked by using a different cost function. One possibility is to use the heat release in Eq. (2.2) integrated over the domain and over time, which will be investigated in a follow-up study.

4. Conclusions and outlook

In this project, we have developed and implemented a gradient-based optimization procedure to identify the 'best' place to ignite a fuel-oxidizer mixture. We have used the time-averaged increase in thermal energy as the cost function that indicates the success of ignition. We have used the unsteady adjoint of the nonlinear LMN equations to obtain sensitivity gradients of the cost function with respect to the position of the spark. We used this technique to study an axisymmetric jet diffusion flame. We found that the optimal locations track the stoichiometric mixture fraction surface in the flow. In this study, we have fixed the shape of the initial condition and optimized the location. A natural extension is to allow the shape to vary and find the optimal initial condition of fixed energy. This could lead to insights into new approaches for ignition.

The techniques developed here can easily be applied to flows in more complex geometries and flows featuring highly unsteady behavior. To begin with, we will study a lifted jet diffusion flame at Re = 1000. Preliminary results for this flow suggest that the optimization procedure finds multiple local optimals, in this case at $(3.03, 0.63)$ and $(5.53, 0.65)$. It remains to be seen whether these lead to flames with different lift-off heights.

Acknowledgments

REFERENCES

CAPECELATRO, J., VISHNAMPET, R., BODONY, D. J. & FREUND, J. B. 2016 Adjoint-based sensitivity analysis of localized ignition in a non-premixed hydrogen–air mixing layer. In *54th AIAA Aerospace Sciences Meeting*, p. 2153.

CHANDLER, G. J., JUNIPER, M. P., NICHOLS, J. W. & SCHMID, P. J. 2012 Adjoint algorithms for the Navier-Stokes equations in the low Mach number limit. *J. Comput. Phys.* **231**, 1900–1916.

FOURES, D., CAULFIELD, C. & SCHMID, P. 2013 Localization of flow structures using-norm optimization. *J. Fluid Mech.* **729**, 672–701.

JAMESON, A. 1988 Aerodynamic design via control theory. *J. Sci. Comput.* **3**, 233–260.

JUNIPER, M. P. 2011 Triggering in the horizontal Rijke tube: non-normality, transient growth and bypass transition. *J. Fluid Mech.* **667**, 272–308.

MASTORAKOS, E. 2009 Ignition of turbulent non-premixed flames. *Prog. Energ. Combust.* **35**, 57 – 97.

NICHOLS, J. W. & SCHMID, P. J. 2008 The effect of a lifted flame on the stability of round fuel jets. *J. Fluid Mech.* **609**, 275–284.

PRINGLE, C. C. T. & KERSWELL, R. R. 2010 Using nonlinear transient growth to construct the minimal seed for shear flow turbulence. *Phys. Rev. Lett.* **105**, 154502.

QADRI, U. A., CHANDLER, G. J. & JUNIPER, M. P. 2015 Self-sustained hydrodynamic oscillations in lifted jet diffusion flames: origin and control. *J. Fluid Mech.* **775**, 201–222.

RICHARDSON, E. S. & MASTORAKOS, E. 2007 Numerical investigation of forced ignition in laminar counterflow non-premixed methane-air flames. *Combust. Sci. Technol.* **179**, 21–37.